August 2020
Master's Degree Thesis

High Precision Sensorless Speed Control of SPMSM based on Adaptive Observer utilizing Predictive Approach

Graduate School of Chosun University

Department of Electrical Engineering

Muhammad Usama

High Precision Sensorless Speed Control of SPMSM based on Adaptive Observer utilizing Predictive Approach

예측제어 기반의 적응형 관측기를 이용한 표면 부착형 영구자석 동기모터의 고정밀 센서리스 속도제어

2020 년 8 월 28 일

Graduate School of Chosun University

Department of Electrical Engineering

Muhammad Usama

High Precision Sensorless Speed Control of SPMSM based on Adaptive Observer utilizing Predictive Approach

Advisor: Prof. Jaehong kim

A thesis submitted in partial fulfilment of the requirements for a Master's degree

May 2020

Graduate School of Chosun University

Department of Electrical Engineering

Muhammad Usama

우사마 무함마드 벌더의 석사학위 논문을

인준함

위원장 조선대학교 교수 김용재㊞

위 원 조선대학교 교수 최연옥㊞

위 원 조선대학교 교수 김재홍㊞

2020년 06월

조선대학교 대학원

TABLE OF CONTENTS

LIST OF ABBREVIATIONS AND ACRONYMS

SPMSM	Surface-Mount Permanent Magnet Synchronous Motor
PI	Proportional Integral
VV	Voltage Vector
MRAS	Model Reference Adaptive System
FCS-MPCC	Finite Control Set-Model Predictive Current Control
MPTC	Model Predictive Torque Control
SMO	Sliding Mode Observer
EMF	Electromotive Force
DTC	Direct Torque Controller
FOC	Field Oriented Control
VSI	Voltage Source Inverter
MTPA	Maximum Torque per Armature

List of Figures

List of Tables

ABSTRACT

High Precision Sensorless Speed Control of SPMSM based on Adaptive Observer utilizing Predictive Approach

Muhammad Usama
Advisor: Prof. Jaehong Kim, Ph.D.
Department of Electrical Engineering
Graduate School of Chosun University

The objective of the paper is to present the efficient and dynamic sensorless speed control of a nonsilent permanent magnet synchronous motor (SPMSM) drive at a wide speed range. For high-performance speed sensorless control, a finite control set model predictive current control (FCS-MPCC) algorithm based on a model reference adaptive system (MRAS) is proposed. With the FCS-MPCC algorithm, the inner current control loop is eliminated, and the limitations of the cascaded linear controller are overcome. The proposed speed sensorless control algorithm provides an efficient speed control technique for the SPMSM drive owing to its fast dynamic response and simple principle. The adaptative mechanism is adopted to estimate the rotor shaft speed and position used in FCS-MPCC for dynamic sensorless control. FCS-MPCC uses a square cost function to determine the optimal output voltage vector from the switching states that give the low cost index. A discrete-time model of a system is used to predict future currents across all the feasible voltage vector produced by the voltage source inverter. The optimal voltage vector that reduced the cost function is adopted and utilized. Simulation results showed the efficacy of the presented scheme and the

viability of the proposed sensorless speed control approach under diverse loading conditions at wide speed operation range.

한 글 요 약

예측제어 기반의 적응형 관측기를 이용한 표면 부착형 영구자석 동기모터의 고정밀 센서리스 속도제어

우사마 무하마드
지도 교수: 김재홍
전기 공학과
대학원, 조선대학교

본 논문에서는 표면 부착형 영구자석 동기모터(Surface-mounted permanent-magnet synchronous machine: SPMSM)를 넓은 속도범위에서 효과적으로 센서리스 속도제어 하는 방법을 제안하였다. 고성능 센서리스 속도제어를 위해, 모델참조 적응시스템(Model reference adaptive system: MRAS)을 기반으로 한 유한 제어집합 모델예측 전류제어(Finite set model predictive current control: FCS-MPCC) 알고리즘을 제안하였다. 내부 전류제어 루프가 FCS-MPCC로 대체되었고, 따라서 직렬로 연결된 선형제어기의 한계를 극복하였다. 제안된 센서리스 제어 알고리즘을 사용하면 빠른 동적응답과 간단한 구현방법 덕분에 SPMSM을 효과적으로 속도제어 할 수 있다. 적응 매커니즘은 센서리스 제어를 위한 FCS-MPCC에서 회전자축의 속도 및 위치를 추정하는데 사용되었다. 이 FCS-MPCC는 비용지수를 최소로 만드는 스위칭 상태로부터 최적의 출력전압 벡터를 결정하기 위해 제곱 비용함수의 형태를 적용하였다. 또한, 시스템의 이산시간 모델은 전압형 인버터에서 사용 가능한 모든 전압벡터에 의한 미래의 전류값를 예측하는데 사용되었다. 본 논문에서 주어진 시뮬레이션 결과는 넓은 속도영역에서 다양한 부하조건에 대해 제안된 센서리스 속도제어 방식이 빠르고 효과적으로 동작함을 보여준다.

I. INTRODUCTION

A. Power Inverter

Power electronic is the application of solid-state electronics to control and convert electrical power. Electronic devices provide interface between two electrical systems, e.g. conversion of ac to dc.With the advancement in semiconductor technology, the speed control of ac motor drive becomes easy. Inverter with semiconductor switches (MOSFET, IGBT, etc.) creates variable frequency from the direct current source which is further utilized to drive ac motor drive. The two types of inverter exist with different structure and totally different behaviour depend on input source.Based on working principle both the inverter type are different [1]-[2]. Voltage source inverter operates on current control mode fed by stiff dc voltage whereas the current source inverter operates on voltage control mode fed by the stiff current source. Different inverter consisting of six switched and a dc source is shown in Fig. 1.

In voltage source inverter both the parallel connected switches can't operate at same time due to DC-link short circuit. Each switch with anti-parallel diode in voltage source inverter provides commutation path for inductive loads. The traditional current source inverter affect from disadvantages such as harmonic resonance, low speed steady state error and torque pulsation. So, keeping these drawback in mind the voltage source inverters are utilized in this paper.

B. Literature Review

Recently surface-mounted permanent magnet synchronous motor (SPMSM) drives have attracted increased attention for industrial applications in variable

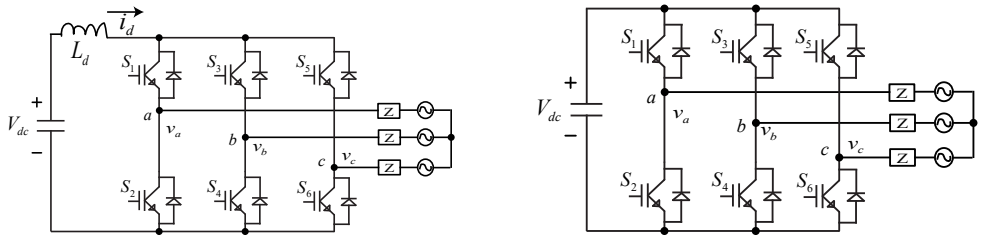

(a) Current source inverter (b) Voltage source inverter

Figure 1: Three-phase inverter

speed control systems. SPMSM drives replace asynchronous and dc motor drives in various industrial sectors owing to advantages, such as small size, high power-to-size ratio, zero copper loss across the secondary winding, high efficiency, simple modeling, low maintenance cost, and high power factor [3]. For applications in hybrid electric vehicles, ships, and elevators, SPMSM drives need high-performance control and high efficiency for quick dynamic response and accurate position tracking [4]. For high-performance control, mechanical sensors are used to sense the rotor shaft speed and position; however, such sensors can be affected by the environment as well as increase the price of the system and decrease system reliability. Owing to these factors, the development of sensorless speed and position control technology has become important [5]-[6]. Different sensorless control schemes had been proposed as shown in Fig.2, including model-based sensorless approaches and high-frequency signal injection schemes [7]-[8]. Among the model-based sensorless approaches non adaptive methods use measured motor phase current and voltage as well as fundamental machine equations of motor drive. These methods are easy to compute, simple to implement with give quick response but on contrary these methods require accurate motor parameters and give erroneous results with

parameter perturbation.

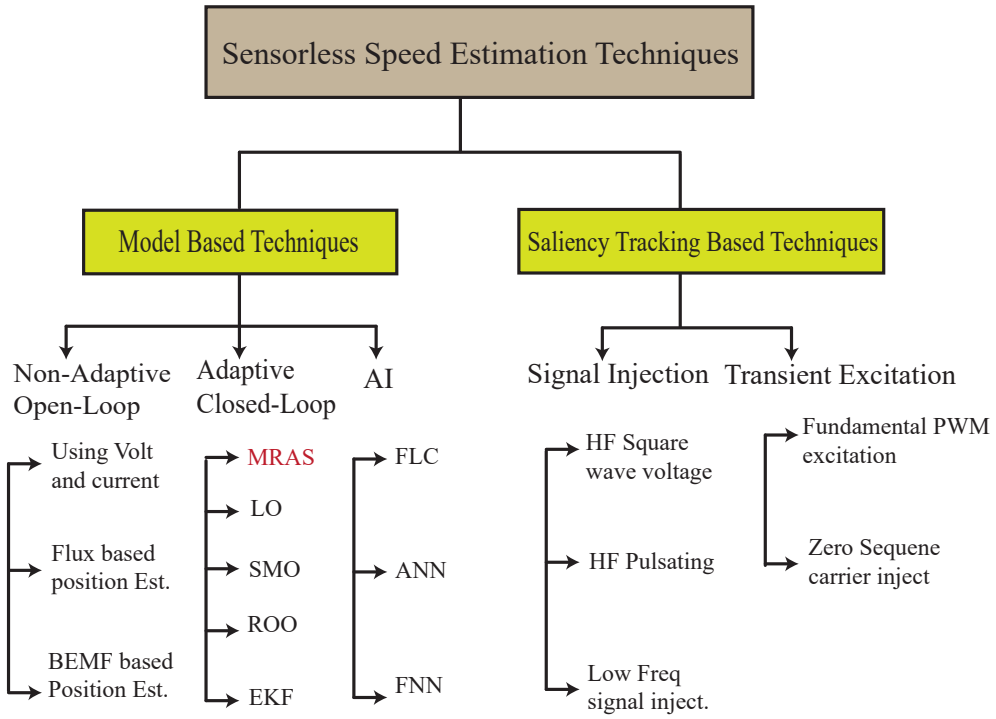

Figure 2: Sensorless techniques.

Among adaptive techniques,sliding mode observer are most popular and widely used because of its easy implementation and zero effect on parameter perturbation. However, the major disadvantage of this approach is that it is not effective in the low or zero speed range because the estimation is based on electromagnetic field (EMF) signals that contain information of shaft speed and position. Thus, at low or zero speed where there is no EMF information, the estimation of a sensorless algorithm is not possible [9]. The fuzzy control scheme is designed to deal with the non-linearity of SPMSM by utilizing inference rules; however, it requires extensive knowledge and experience in determining

the rules [10]. Saliency based technique is mostly employed for motor drive having saliency like IPMSM. High frequency signal is injected in motor drive terminal with main driving power. The high frequency signal will not affect the motor motion but will yield different response of dq-axis current due to rotor misalignment and that is cause because of rotor saliency. Based on this real rotor position is observed and this technique help to estimate the rotor speed at low speed or standstill.

Due to non-salient motor drive, the adaptive control model is design to estimate the rotor speed at low or negative operation range. The model reference adaptive control technique is employed to design a sensorless speed control model. The model reference adaptive system (MRAS)-based control approach has been studied by various researchers. It utilizes proportional-integral (PI)-based cascade loop control for sensorless control of SPMSMs. The MRAS performs efficiently in the low- and high-speed operation region. However, its performance is restricted by motor parameter uncertainties, although encoder-less speed control can still be achieved. The MRAS with an inner current control loop with PI gain increases both the speed ripple and rise time with large overshoot [11]-[12].

In a recent years,model predictive control (MPC) has emerged as a powerful control method for the efficient dynamic performance of motor drives and power converters. Predictive controller is a non-linear controller that uses the model of the system to predict the future states and control variable of the system. Various classifications are made based on which different predictive control techniques are shown in Fig.3.

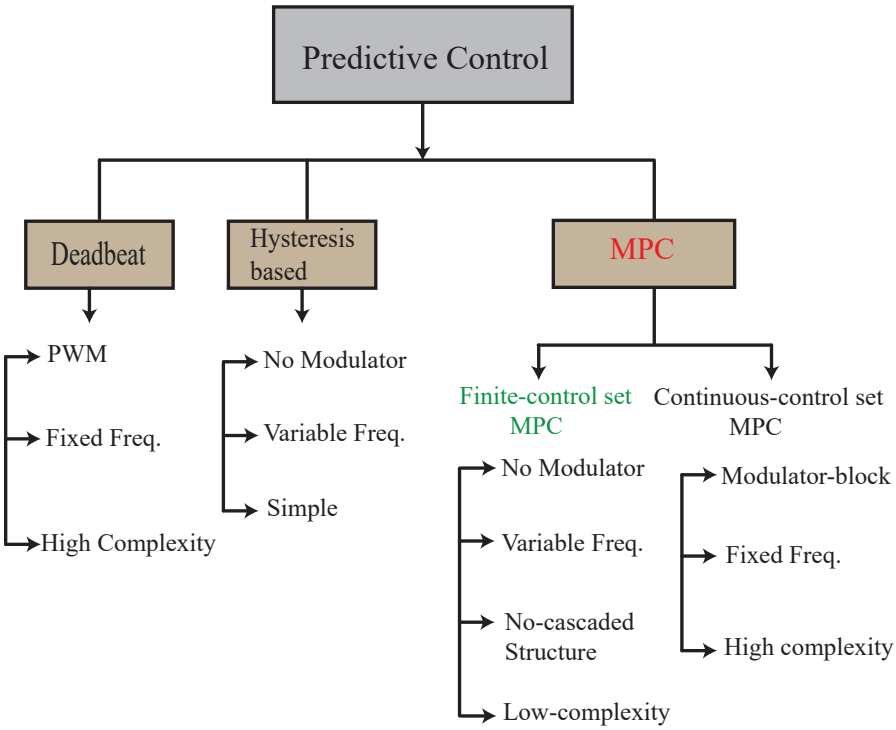

Figure 3: Various predictive control designs.

The most common predictive control strategies are Hysteresis control, deadbeat control and model predictive control. Hysteresis based controller maintain the control variable with in a given hysteresis band and is simple and easy to implement and is also known as bang bang controller but for efficient response hysteresis band need to be small that cause high switching loss. In deadbeat, the system equation is employed to reach to reference current value based on voltage vector applied. Deadbeat controller are sensitive to model parameter error and system delay that affect the system performance. Continuous predictive control utilized the average model of the system and has complex

optimization process. So finite control set mpc is proposed with square cost function to estimate the future state of the system based on input control variables.

Compared with conventional control methods, such as field-oriented control(FOC) and direct torque control (DTC), the FCS-MPC scheme shows high performance because it is based on the internal model of the motor drive. In FOC, the fine-tuning of PI gain is required, which is a major concern, and the current control loop bandwidth is limited, These problems make FOC unsuitable for high dynamic response applications. In DTC, the current control loop is eliminated along with modulation block. The optimal output VV is chosen based on a lookup table designed according to the flux and torque difference and stator flux position. DTC causes high ripples across the torque and phase current [13]-[14]. MPC employs the discrete-time function of a system to predict the future response over the discrete instant, and adopts suitable control measures according to a predefined cost function [15]. With the limited number of possible switching configurations of the voltage source inverter (VSI), the optimal output VV is determined, and shows the efficient current control technique for different types of power inverters for motor drive applications [16]. Model predictive torque control (MPTC) shows good response to torque ripple and motor phase current harmonics, in contrast to conventional DTC. The optimal VV is obtained by combining the torque and flux errors into a cost function to evaluate the error and provide the optimal output VV. However, owing to different units of torque and flux, a special step is required when selecting the weighting factor of the stator flux, which requires fine-tuning and makes MPTC unsuitable [17]. In (MPCC), the phase current is the only control variable taken into account for error evaluation across the cost function or decision function for the optimal output VV. MPCC has a simple principle and solution compared with MPTC

because the phase current is only a control variable that is easily measured across the motor drive [18]-[19].

C. Thesis Objective

In this thesis, the possible switching configurations of the VSI are considered, and the pulse modulation block method is eliminated. A squared cost function is proposed for efficient reference quadrature axis i_q^* current tracking and dynamic performance. Hybrid method is employed as alternative approach to enhance the sensorless control performance of motor drive. As in SPMSM torque is directly dependent on stator current, so therefore instantaneous motor phase current with high accuracy and short transient period together with high high performance and low harmonic can potentially improve overall torque performance. The main contribution of this paper is improvement of the dynamic response of motor drives for sensorless speed control applications at a wide speed range under variable loading conditions by designing an MRAS estimator for continuously estimating the rotor shaft angular velocity and position. and used the estimating values online in (FCS-MPCC) for estimating the optimal output VV for the VSI. In this thesis, FCS-MPC approach is introduced along with the estimation algorithm based on the adaptative mechanism for sensorless speed control rather then traditional PI-MRAS control. With the MRAS based on FCS-MPCC, the efficiency of the ac motor drive improved significantly with fast dynamic response and reduced ripple across the shaft speed.

The literature review and thesis goal are mentioned in chapter I. The mathematical model of the SPMSM is described in Chapter II. In Chapter III, the proposed algorithm for sensorless speed control along with stability analysis

is presented. The development of the proposed design and the verification of sensorless speed control under transient conditions are described in Chapter IV. The conclusion is given in Chapter V.

II. Modelling of SPMSM

Permanent Magnet (PMs)eliminate the use of field exciting coils and slip ring for current conduction. Due to the absence of field winding inside the rotor, PM motors have low inertia. The field strength is so high such that the volume of the motor reduced. As there is no copper loss of the secondary winding, the PM motors have high efficiency and dynamic performance than induction motors [3].

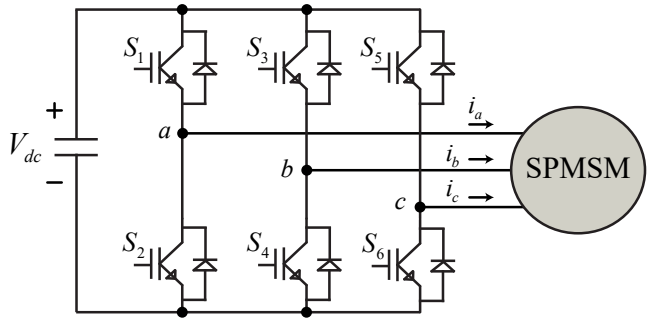

Figure 4: Three-phase two-level VSI-fed SPMSM.

For industrial applications, a two-level VSI is the best choice because it is simple to design and is economical. The two-level three-phase inverter connected to the SPMSM is shown in Fig. 4. V_{dc} is the VSI input voltage, and voltage $\mathbf{v}_{abc}$ is applied across the SPMSM windings. The six switches of the VSI shape the output voltages that are controlled by the switching pulse order given by the MPCC.

The dq-equivalent circuit of SPMSM is shown in Fig. 5. In a three-phase

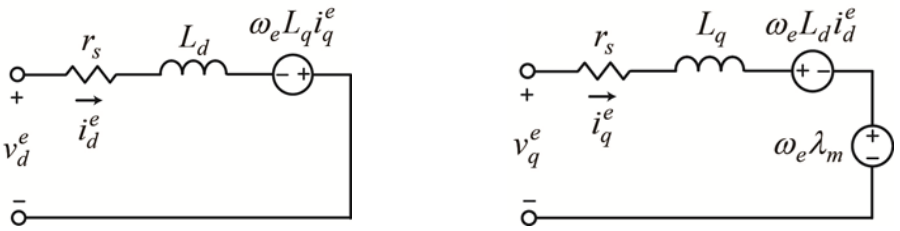

(a) d-axis (b) q-axis

Figure 5: SPMSM equivalent circuit.

coordinate system, the voltage equations of SPMSM is given as [3]

$$\begin{bmatrix} v_a \\ v_b \\ v_c \end{bmatrix} = r_s \begin{bmatrix} i_a \\ i_b \\ i_c \end{bmatrix} + \frac{d}{dt} \begin{bmatrix} \lambda_a \\ \lambda_b \\ \lambda_c \end{bmatrix}. \tag{1a}$$

$$\begin{bmatrix} \lambda_a \\ \lambda_b \\ \lambda_c \end{bmatrix} = \begin{bmatrix} L_{ms}+L_{ls} & -\frac{1}{2}L_{ms} & -\frac{1}{2}L_{ms} \\ -\frac{1}{2}L_{ms} & L_{ms}+L_{ls} & -\frac{1}{2}L_{ms} \\ -\frac{1}{2}L_{ms} & -\frac{1}{2}L_{ms} & L_{ms}+L_{ls} \end{bmatrix} \begin{bmatrix} i_a \\ i_b \\ i_c \end{bmatrix} + \lambda_m \begin{bmatrix} cos\theta_r \\ cos\theta_r - \frac{2\pi}{3} \\ cos\theta_r + \frac{2\pi}{3} \end{bmatrix}. \tag{1b}$$

$$v_d = r_s i_d + \frac{d\lambda_d}{dt} - \omega_r \lambda_q. \tag{1c}$$

$$v_q = r_s i_q + \frac{d\lambda_q}{dt} + \omega_r \lambda_d. \tag{1d}$$

$$\lambda_d = L_s i_d + \lambda_m. \tag{1e}$$

$$\lambda_q = L_s i_q. \tag{1f}$$

$(1b)$ is the stator flux linkage equation that is determined in [3], where L_{ms} is the mutual inductance between the windings, L_{ls} is the self inductance of stator winding and λ_m is the permanent magnet flux. The total stator flux linkage is the combination of stator current and rotor flux. SPMSM are considered to have

uniform airgap from the view of magnetic circuit of stator winding, since the permeability of permanent magnet is close to one the inductance is constant and is independent of rotor position. The PMSM model is simplified by transforming the three phase voltage *abc* reference $(1a)$ to d-q synchronous reference frame with the well-known Park's transformation and obtained as (1c) and (1d). The dq-model in synchronous frame is shown in Fig. 6. Flux linkage dq components are obtained by transforming stator flux linkage $(1b)$ to synchronous reference frame.

The voltage equation of SPMSM in synchronous reference frame using (1) can be written:

$$\begin{bmatrix} v_d^e \\ v_q^e \end{bmatrix} = \begin{bmatrix} r_s + L_s p & -\omega_r L_s \\ \omega_r L_s & r_s + L_s p \end{bmatrix} \begin{bmatrix} i_d^e \\ i_q^e \end{bmatrix} + \begin{bmatrix} 0 \\ \omega_r \lambda_m \end{bmatrix}. \tag{2}$$

where r_s is the stator resistance, λ_m is the rotor flux linkage, ω_r is the electrical rotor speed, and p is a differential operator. As SPMSM is nonsilent and independent of rotor position so, $L_s = L_d = L_q$. Then, the electromagnetic torque T_e generated by the motor is given as:

$$T_e = \frac{3P}{2}(\lambda_d^e i_q^e - \lambda_q^e i_d^e) \tag{3a}$$

$$T_e = \frac{3P}{2}[\lambda_m i_q^e - (L_q - L_d) i_d^e i_q^e] \tag{3b}$$

$$T_e = \frac{3P}{2}[\lambda_m i_q^e]. \tag{3c}$$

where P is the poles pair. The mechanical equation is

$$T_L = T_e - B\omega_m - Jp\omega_m. \tag{4}$$

where T_L is the load torque, ω_m is the rotor mechanical speed, and J and B are the motor inertia and friction coefficient, respectively. The relationship between

mechanical and electrical rotor position is $\theta_r = P\theta_m$. Based on (2-4) the PMSM dynamic model is shown in Fig. 8.

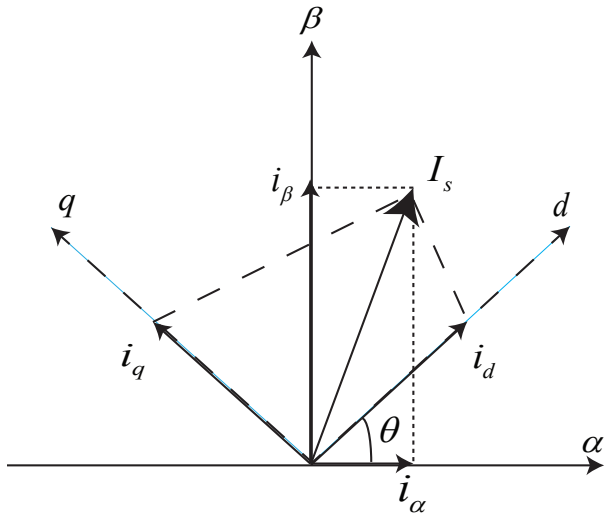

Figure 6: View of dq-axis SPMSM.

From (2), the dynamic dq current model of SPMSM is obtained as

$$\frac{d}{dt}\begin{bmatrix} i_d^e \\ i_q^e \end{bmatrix} = \begin{bmatrix} -\frac{r_s}{L_s} & \omega_r \\ -\omega_r & -\frac{r_s}{L_s} \end{bmatrix}\begin{bmatrix} i_d^e \\ i_q^e \end{bmatrix} + \begin{bmatrix} \frac{1}{L_s} & 0 & 0 \\ 0 & \frac{1}{L_s} & -\frac{\lambda_m}{L_s} \end{bmatrix}\begin{bmatrix} v_d^e \\ v_q^e \\ \omega_r \end{bmatrix}. \quad (5)$$

$\mathbf{i}_{dq}^e = [i_d^e \; i_q^e]^T$ is the system output, whereas $\mathbf{v}_{dq}^e = [v_d^e \; v_q^e]^T$ is the control input in (5). The dq-transformation simulink model is shown in Fig.7

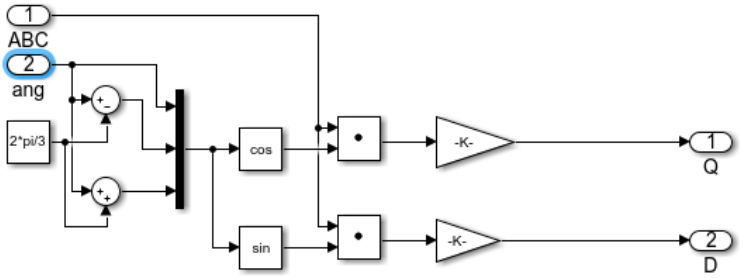

Figure 7: DQ-transformation.

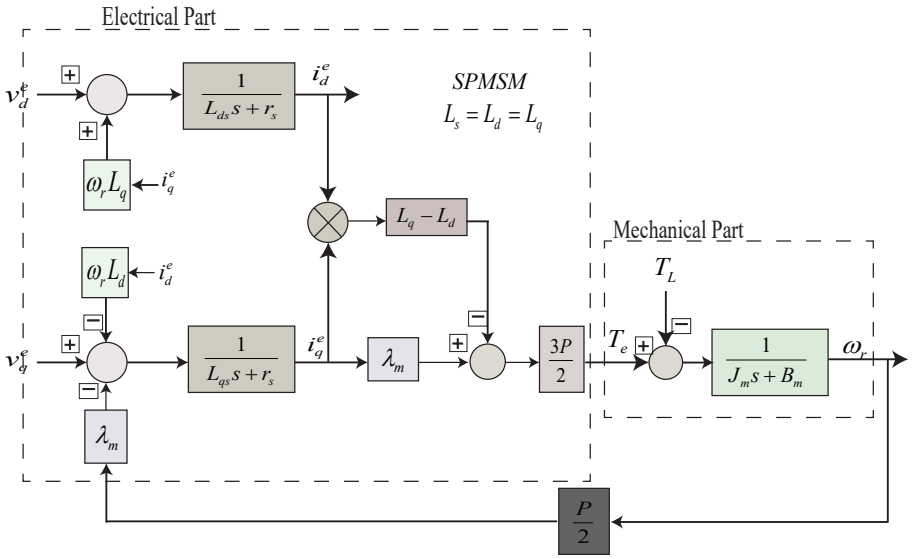

Figure 8: PMSM dynamic model.

III. Proposed Speed Sensorless Control Algorithm

In this section, the speed sensorless control algorithm is described in detail. In traditional sensorless control design the classical fixed PI current controllers are employed. The output of PI current controllers are the voltages which are used to obtain switching pulse for VSI based on modulation technique. The classical fixed gain PI current controllers are sensitive to parameter variation along with reference speed and load disturbance. secondly the due to cascaded structure the gain value are selected such that the closed loop bandwidth is larger than the speed bandwidth. Due to these limitations, the nonlinear current controller for sensorless speed operation is proposed to increase the efficiency and performance under the load conditions. The proposed design is structured as: First, the discrete-time model of the SPMSM is described. Then, the FCS-MPCC is discussed, which generates the switching pulse for the VSI to control the reference model of the algorithm. Finally, the MRAS-based sensorless control approach is applied to estimate the motor angular velocity and position for dynamic control of the motor drive.

A. Discrete Model of SPMSM drive

MPC method uses the discrete-time model of the system to predict the future value of load current for each possible VV. The mathematical model of SPMSM is discretize to determine the necessary condition for model prediction. An internal discrete-time model of the motor drive was utilized to predict the future state of the output state variable for input control over the sample time T_s. The discrete-time internal model of the motor drive was obtained by forward Euler

approximation, which is written as follows [20]:

$$\frac{di}{dt} \approx \frac{[i^{k+1} - i^{k}]}{T_s}. \tag{6}$$

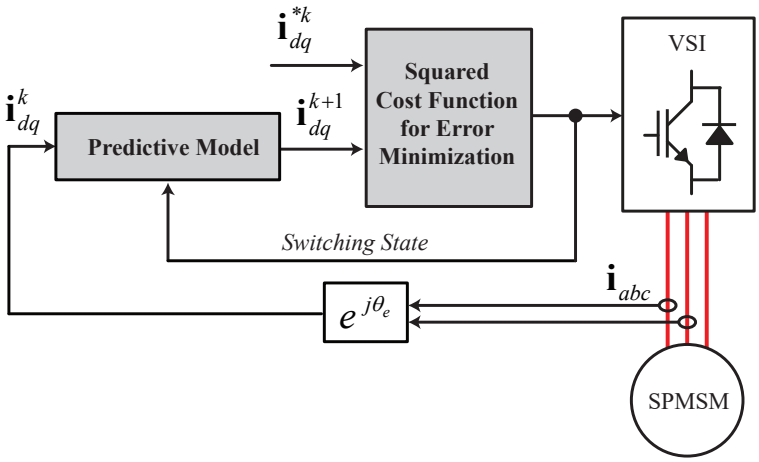

Figure 9: MPCC technique for SPMSM.

The predictive current control also examined the three-phase two-level inverter model to determine the optimal output VV. The states of the inverter switches are listed in Table. 1 and utilized in Fig. 9. The three-phase inverter is described by

$$S = \frac{2}{3}(S_1 + e^{j\frac{2\pi}{3}} S_3 + e^{j\frac{4\pi}{3}} S_5). \tag{7}$$

The motor phase voltages calculated by the switching states of VSI are expressed as follows:

$$\begin{bmatrix} v_{as} \\ v_{bs} \\ v_{cs} \end{bmatrix} = \frac{V_{dc}}{3} \begin{bmatrix} 2 & -1 & -1 \\ -1 & 2 & -1 \\ -1 & -1 & 2 \end{bmatrix} \begin{bmatrix} S_1 \\ S_3 \\ S_5 \end{bmatrix}, \tag{8}$$

where V_{dc} is the inverter input dc voltage, as shown in Fig. 4. With the possible combinations of switching patterns, the output VVs are acquired. Thus, three-phase motor voltages are transformed into rotor reference frames by utilizing well known Park's transformation as

$$\begin{bmatrix} v_d^e \\ v_q^e \\ v_0^e \end{bmatrix} = \frac{2}{3} \begin{bmatrix} cos\theta_r & cos(\theta_r - \frac{2\pi}{3}) & cos(\theta_r + \frac{2\pi}{3}) \\ sin\theta_r & sin(\theta_r - \frac{2\pi}{3}) & sin(\theta_r + \frac{2\pi}{3}) \\ \frac{1}{\sqrt{2}} & \frac{1}{\sqrt{2}} & \frac{1}{\sqrt{2}} \end{bmatrix} \begin{bmatrix} v_{as} \\ v_{bs} \\ v_{cs} \end{bmatrix}. \tag{9}$$

By Euler forward approximation, (2) can be expressed in the discrete-time model as

$$v_d^k = r_s i_d^k + \frac{L_s}{T_s}(i_d^{k+1} - i_d^k) - \omega_r^k L_s i_q^k, \tag{10}$$

$$v_q^k = r_s i_q^k + \frac{L_s}{T_s}(i_q^{k+1} - i_q^k) + \omega_r^k L_s i_d^k + \omega_r^k \lambda_m. \tag{11}$$

Therefore, the discrete-time current model of the motor drive is derived from (10) and (11), and given as

$$i_d^{k+1} = i_d^k + \frac{T_s}{L_s}(-r_s i_d^k + \omega_r^k L_s i_q^k + v_d^k), \tag{12}$$

$$i_q^{k+1} = i_q^k + \frac{T_s}{L_s}(-r_s i_q^k - \omega_r^k L_s i_d^k - \omega_r^k \lambda_m + v_q^k). \tag{13}$$

where $\mathbf{i}_{dq}^k$ are the measured output state variables at K^{th} sampling instant; i_{dq}^{k+1} are the predicted output state variables at the $k+1$ sampling period; and $\mathbf{v}_{dq}^k$ are the control input variables that must be selected based on the inverter switching state. The motor speed is considered constant at several control instances as the electromechanical time constant of the motor drive is lower than the mechanical time constant, which shows $\omega_r^{k+1} \approx \omega_r^k$ [21]. The rotor flux was calculated from (3c) as saturation or temperature uncertainty may affect performance.

Table 1: Inverter switching configuration.

Inverter On Legs	Voltage Vector	Switching States		
		S1	S3	S5
S_2, S_4, S_6	v_0=0	0	0	0
S_2, S_4, S_5	v_1=$\frac{2}{3}V_{dc}e^{j\frac{4\pi}{3}}$	0	0	1
S_2, S_3, S_6	v_2=$\frac{2}{3}V_{dc}e^{j\frac{2\pi}{3}}$	0	1	0
S_2, S_3, S_5	v_3=$\frac{2}{3}V_{dc}e^{j\pi}$	0	1	1
S_1, S_4, S_6	v_4=$\frac{2}{3}V_{dc}$	1	0	0
S_1, S_4, S_5	v_5=$\frac{2}{3}V_{dc}e^{j\frac{5\pi}{3}}$	1	0	1
S_1, S_3, S_6	v_6=$\frac{2}{3}V_{dc}e^{j\frac{\pi}{3}}$	1	1	0
S_1, S_3, S_5	v_7=0	1	1	1

B. Finite Control Set Model Predictive Current Control

MPC approaches have recently been observed in different industrial applications owing to their rapid dynamic response and efficient control performance compared with other control mechanisms. The structure of the FCS-MPCC for the SPMSM drive is shown in Fig. 9. An important part of MPC is the selection of the cost function to determine the optimal output VV. This is obtained in a way that minimizes the cost function. The flow diagram of predictive current controller is depicted in Fig. 10. As $\mathbf{i}_{dq}^{k}$ are directly controlled in FCS-MPCC, the square cost function can be selected as

$$g = (i_d^{*k} - i_d^{*(k+1)})^2 + (i_q^{*k} - i_q^{*(k+1)})^2. \tag{14}$$

where $\mathbf{i}_{dq}^{*k}$ are the reference current values in the synchronous reference frame. A speed regulator was employed at the outer loop to generate the quadrature

reference current i_q^{*k}, while the direct reference current i_d^{*k} was set to zero to determine maximum torque per ampere control (MTPA). The VV for the motor drive was selected based on the square cost function. The switching states in Table. 1 were applied across the inverter, which caused the applied motor phase current to reach the reference current value in the next sampling period, after the cost function was minimized [19]. As a result, the predictive current was applied across the motor drive and operated according to the reference current value.

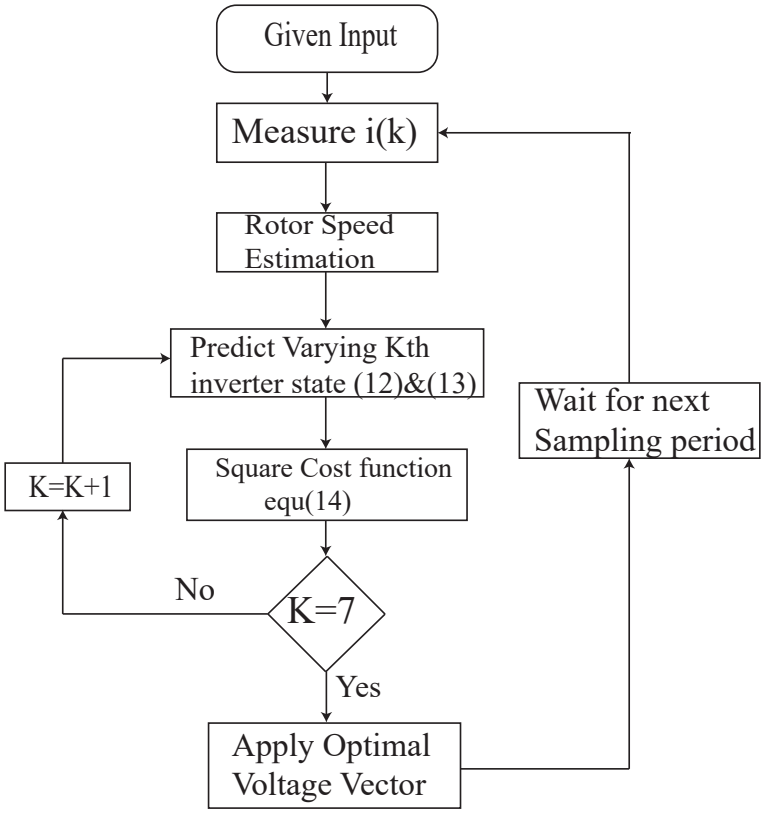

Figure 10: Flow diagram of current control technique.

The control method of the given MPCC has two main parts. First, it

determines the optimal output VV that yields the lowest cost index. Second, it defines the duration of output VV application in the next control period to minimize the cost index. In two-level three-phase VSIs, there are eight switching configurations with VVs $\mathbf{V}_0, \mathbf{V}_1, ..., \mathbf{V}_7$, as shown in Table. 1. In order to find the optimal output VV, $\mathbf{v}_{dq}^k$ should be selected based on the actual phase voltage and switching equation given in (8) to obtain a predicted current value that reduces the cost index. It is possible to predict the current value in the next sampling period utilizing (12-13). As the input control variable $\mathbf{v}_{dq}^k$ depends on the rotor speed as given in (10-11), the discrete state-space model of SPMSM becomes nonlinear. For sensorless control, shaft speed was estimated using the adaptive mechanism and applied in MPC. The feasibility of the rotor shaft speed for a given $\mathbf{i}_{dq}^k$ could be determined based on the input variable $\mathbf{v}_{dq}^k$ with the availability of optimal output VV. From Table. 1, the possibility of input variable $\mathbf{V}_{dq}^k$ can be obtained in terms of the inverter input voltage. Once the optimal output VV is selected, the pulse order for insulated-gate bipolar transistor (IGBT) switches of VSI is generated.

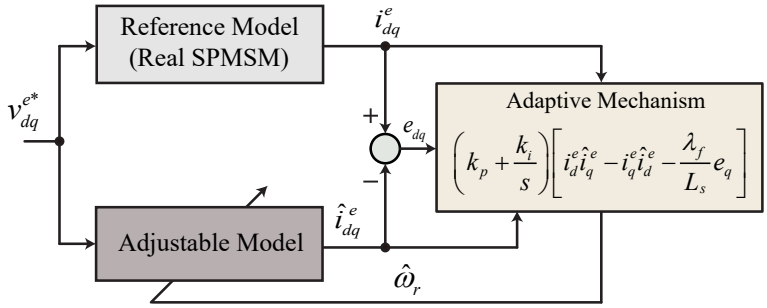

Figure 11: SPMSM speed estimation structure based on MRAS.

C. MRAS-Based Adaptive Estimation

MRAS is an adaptive control system in which the desired performance of the motor drive is expressed in terms of a reference model, which offers the desired response to a command signal [22]. The MRAS estimator are built to estimate the dq axis stator phase current and rotor shaft speed. MRAS is a simple approach to implement and can reduce the computational processing time. Fig. 11 shows the MRAS structure for estimating rotor shaft speed. The estimated shaft speed will track the actual shaft speed based on adaptive rule. Then, the rotor shaft position was obtained by integrating the estimated shaft speed. According to MRAS, two models were selected based on their physical meaning. One is the reference model with definite motor parameters, while the other is an adjustable model designed based on the fundamental model of a motor drive.

$$\frac{d}{dt}\begin{bmatrix} \hat{i}_d^e \\ \hat{i}_q^e \end{bmatrix} = \begin{bmatrix} -\frac{r_s}{L_s} & \hat{\omega}_r \\ -\hat{\omega}_r & -\frac{r_s}{L_s} \end{bmatrix}\begin{bmatrix} \hat{i}_d^e \\ \hat{i}_q^e \end{bmatrix} + \begin{bmatrix} \frac{1}{L_s} & 0 & 0 \\ 0 & \frac{1}{L_s} & -\frac{\lambda_m}{L_s} \end{bmatrix}\begin{bmatrix} v_d^e \\ v_q^e \\ \hat{\omega}_r \end{bmatrix}. \tag{15}$$

The current model of the SPMSM contains information on rotor speed as given in (15), which is used as an adaptable model, while the motor drive itself (5) is considered as the reference model. Both models have the same physical meaning with same inputs $\mathbf{v}_{dq}^e$ and state outputs $\mathbf{i}_{dq}^e$. The outputs of the two models were compared in the adaptation mechanism to estimate the adjustable parameters that tune the adjustable model, in order to reduce the output error between these models to zero.

From (5) the state space dq axis current of SPMSM design as reference model

is given by:

$$\frac{dx}{dt} = Ax + Bu \tag{16}$$

where

$$\mathbf{x} = \begin{bmatrix} i_d^e \\ i_q^e \end{bmatrix}, \mathbf{u} = \begin{bmatrix} v_d^e \\ v_q^e \\ \omega_r \end{bmatrix}, \mathbf{A} = \begin{bmatrix} -\frac{r_s}{L_s} & \omega_r \\ -\omega_r & -\frac{r_s}{L_s} \end{bmatrix},$$

$$\mathbf{B} = \begin{bmatrix} \frac{1}{L_s} & 0 & 0 \\ 0 & \frac{1}{L_s} & \frac{\lambda_m}{L_s} \end{bmatrix}.$$

The state space model of SPMSM based on adjustable model is given as:

$$\frac{d\hat{x}}{dt} = \hat{A}\hat{x} + B\hat{u} \tag{17}$$

where

$$\hat{\mathbf{x}} = \begin{bmatrix} i_d^e \\ i_q^e \end{bmatrix}, \hat{\mathbf{u}} = \begin{bmatrix} v_d^e \\ v_q^e \\ \hat{\omega}_r \end{bmatrix}, \hat{\mathbf{A}} = \begin{bmatrix} -\frac{r_s}{L_s} & \hat{\omega}_r \\ -\hat{\omega}_r & -\frac{r_s}{L_s} \end{bmatrix},$$

$$\mathbf{B} = \begin{bmatrix} \frac{1}{L_s} & 0 & 0 \\ 0 & \frac{1}{L_s} & -\frac{\lambda_m}{L_s} \end{bmatrix}.$$

The adaptive mechanism was designed based on the error signal from the MRAS approach. In the equation of state, the reference model (5) and adjustable model (15) are subtracted, and the error is defined as $e_{dq} = \hat{i}_{dq} - i_{dq}$, whereas the speed error is given as $\Delta\omega_r = \hat{\omega}_r - \omega_r$.

$$\frac{d}{dt}e_d = -\frac{r_s}{L_s}e_d + \hat{\omega}_r e_q + \Delta\omega_r i_q, \tag{18}$$

$$\frac{d}{dt}e_q = -\frac{r_s}{L_s}e_q - \hat{\omega}_r e_d - \Delta\omega_r[i_d + \frac{\lambda_m}{L_s}], \tag{19}$$

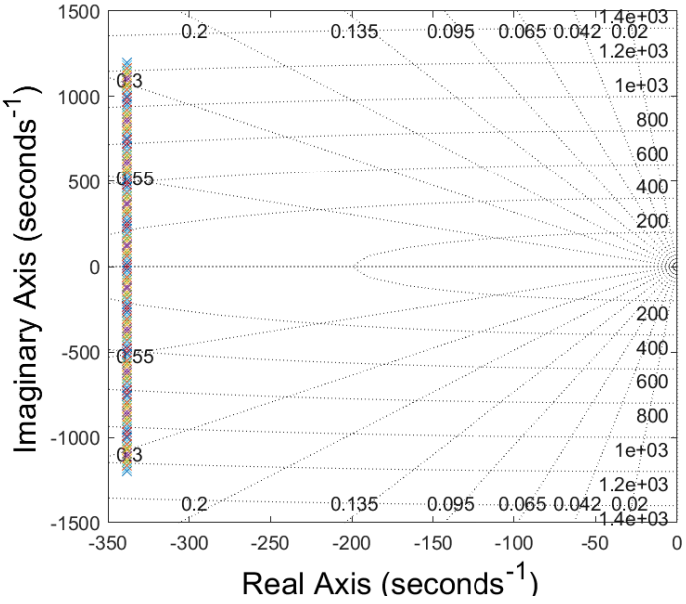

Figure 12: Poles of feedforwad Linear transfer matrix.

$$\frac{d}{dt}\begin{bmatrix} e_d \\ e_q \end{bmatrix} = \begin{bmatrix} -\frac{r_s}{L_s} & \hat{\omega}_r \\ -\hat{\omega}_r & -\frac{r_s}{L_s} \end{bmatrix}\begin{bmatrix} e_d \\ e_q \end{bmatrix} + \Delta\omega_r \begin{bmatrix} -i_q \\ i_d \quad \frac{\lambda_m}{L_s} \end{bmatrix}, \tag{20}$$

The error equation is obtained as

$$\frac{d}{dt}e_{dq} = Ae + W. \tag{21}$$

where e is the error vector $[e_{dq}]^T = [e_d e_q]^T$, **A** is the state matrix, and **W** is the feedback loop output vector given as:

$$\mathbf{A} = \begin{bmatrix} -\frac{r_s}{L_s} & \hat{\omega}_r \\ -\hat{\omega}_r & -\frac{r_s}{L_s} \end{bmatrix}, \mathbf{W} = \begin{bmatrix} -i_q \\ i_d \quad \frac{\lambda_m}{L_s} \end{bmatrix}\Delta\omega_r.$$

Compared with adaptive mechanism design based on Lyapunov stability theorem for which the lyapunov function required using designer's experience. Popov stability criterion are more flexible with simple design approach to obtain the adaptive rule. So compared to conventional adaptive rule design the Popov stability criterion are employed to determine adaptive law. Based on Popov criterion the main steps for designing the adaptive rule are: The MRAC system was transformed into a equivalent system known as nonlinear time-variable feedback system consisting of the nonlinear feedback system and feed-forward linear system. The adaptive rule was designed so that the nonlinear feedback system meets Popov's integral inequality [22]. Design the remaining part of adaptive rule which ensure the strictly positive real of feedforward linear model and transfer the equivalent system to MRAC system. To confirm the stability of the system, two statements should be fulfilled. First and foremost the feedforward linear transfer matrix $G(s)=[Is-A]^{-1}$ should be positive real so that all the poles of the system are on negative half plane. Next, the feedback nonlinear model satisfy the adherent Popov's criterion for stability [23]. The transformation of the MRAS system into the equivalent model is shown in Figure 13. The poles of feedforward linear transfer matrix are shown in Figure 12 for the speed range from -1200 to 1200rpm. The Figure 12 demonstrate that all the poles are placed on negative half plane this ensure, that the first condition for the stability of the system is satisfied.

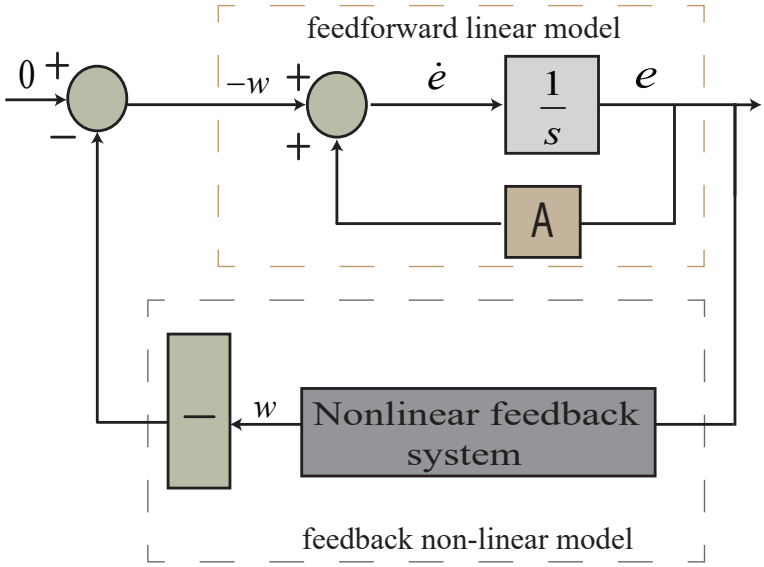

Figure 13: Structure of nonlinear feedback system.

The nonlinear feedback model can be written in form of Popov's integral inequality as [24]

$$\eta(0,t_0) = \int_0^{t_0} e^T W dt \geq -\gamma_0^2, \tag{22}$$

where $t_0 \geq 0$ and γ_0 is a real positive constant independent of t_0. By the conventional form of the adaptive rule, the PI adaptive mechanism is written as [25]

$$\hat{\omega}_r = \int_0^t F_1(t)dt + F_2(t) + \hat{\omega}_r(0). \tag{23}$$

By substituting the value of **W**, the inequality equation (22) becomes

$$\eta(0,t_0) = \int_0^{t_0} [e_d(i_q) + [e_q(-i_d - \frac{\lambda_m}{L_s})]]\Delta\omega_r dt \geq -\gamma_0^2. \tag{24}$$

By utilizing (23), the system becomes

$$\eta(0,t_0) = \int_0^{t_0} [[e_d(i_q) + [e_q(-i_d - \frac{\lambda_m}{L_s})]] \\ [\int_0^t F_1(t)dt + F_2(t) + \hat{\omega}_r(0) - \omega_r]]dt \geq -\gamma_0^2 \tag{25}$$

The above equation is further simplified by splitting it into two parts, given as

$$\eta_{11}(0,t_0) = \int_0^{t_0} [[e_d(i_q) + [e_q(-i_d - \frac{\lambda_m}{L_s})]] \\ [\int_0^{t_0} F_1(t) + \hat{\omega}_r(0) - \omega_r]]dt \geq -\gamma_{11}^2, \tag{26}$$

$$\eta_{12}(0,t_0) = \int_0^{t_0} [[e_d(i_q) + [e_q(-i_d - \frac{\lambda_m}{L_s})]] \\ [F_2(t)]]dt \geq -\gamma_{12}^2, \tag{27}$$

where $\eta(0,t_0) = \eta_{11}(0,t_0) + \eta_{12}(0,t_0)$. By utilizing the Landau relation [26], the solution of abovementioned inequality can be found.

$$\int_0^{t_0} kF(t)\frac{dF(t)}{dt} = \frac{k}{2}[F_{t_0}^2 - F_0^2] \geq \frac{-k}{2} f_{(0)}^2 \\ (k > 0). \tag{28}$$

From above relation (28), the estimated rotor shaft speed satisfies following laws [27]. Consider (26).

$$\frac{dF(t)}{dt} = [e_d(i_q) + [e_q(-i_d - \frac{\lambda_m}{L_s})]], \tag{29}$$

$$kF(t) = [\int_0^{t_0} F_1(t)dt + \hat{\omega}_r(0) - \omega_r], \tag{30}$$

taking the derivative of (30) we get

$$k\frac{dF(t)}{dt} = F_1(t), \tag{31}$$

from (29), we obtained $F_1(t)$ as

$$F_1(t) = k_1[e_d(i_q) + [e_q(-i_d - \frac{\lambda_m}{L_s})]]. \tag{32}$$

Similarly solving for $F_2(t)$, we get

$$F_2(t) = k_2[e_d(i_q) + [e_q(-i_d - \frac{\lambda_m}{L_s})]]. \tag{33}$$

Substituting (32)-(33) in (23), we get the inequality equation (25) in the form of a simplified adaptive rule, where k_1 and k_2 are the positive gains. From Popov's integral inequality theory, we found that when the time approaches infinity, the error will be reduced to zero. Therefore, the adaptive rule(23) for speed estimation based on adaptive observer is asymptotically stable. The estimated shaft speed was obtained from the adaptation mechanism by utilizing the output variable $\mathbf{i}_{dq}^{e}$ of the motor reference and adjustable model; there are errors, as shown in Fig. 11. Finally, the adaptive rule as PI regulator is obtained as

$$\begin{aligned} \hat{\omega}_r = \hat{\omega}_r(0) + K_i \int_0^t [e_d(i_q) + [e_q(-i_d - \frac{\lambda_m}{L_s})]]dt \\ + K_p[e_d(i_q) + [e_q(-i_d - \frac{\lambda_m}{L_s})]] \end{aligned} \tag{34}$$

where K_p and K_i are the speed estimation positive gain value, and $\hat{\omega}_r(0)$ is the initial estimated shaft speed. After solving (34), the rotor shaft speed can be estimated as

$$\hat{\omega}_r = \left[\; K_p + \tfrac{K_i}{s} \; \right] \left[\; i_d\hat{i}_q - i_q\hat{i}_d - \tfrac{\lambda_m}{L_s} e_q \; \right] + \hat{\omega}_r 0 \tag{35}$$

Once the shaft speed is estimated, the shaft position angle can be derived by integration of the estimated shaft speed given as

$$\hat{\theta}_r = \int_0^t \hat{\omega}_r dt \tag{36}$$

The overall sensorless speed control of the proposed approach is shown in Fig. 14. The model was made in Matlab for verification of the proposed method and the feasibility of attaining the desired dynamic response under variable loading conditions. For evaluation the performance of proposed sensorless speed control design, a series of simulations and measurement have been carried out. The dynamic response of design algorithm is evaluated at wide speed range under the transient conditions.

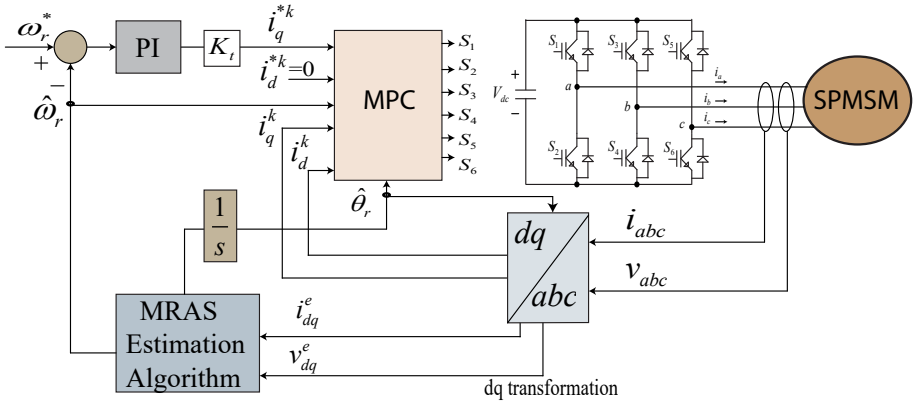

Figure 14: Sensorless speed control scheme based on MRAS utilizing FCS-MPCC.

IV. Results and Discussion

A. Simulation Results

Simulation of the proposed algorithm was carried out utilizing the SPMSM to verify the sensorless operation. The block diagram of the control scheme is shown in Fig. 14. The simulation parameters of the motor drive are listed in Table 2. The optimal PI gain values for speed regulator is given. The outer speed regulator regulates the speed by adjusting the current that passes through the motor as this modifies the torque which in end modifies the speed. The outer speed control loop was utilized to provide i_q^{*k}, while the direct reference i_d^{*k} current was considered as zero. MPCC was utilized to generate the switching pulses for IGBT switches of VSI that determine the shape of the output voltage across the motor. The voltage was then applied to the adjustable model for the estimation algorithm. The measured current from the reference model and estimated current from the adjustable model were used to obtain the estimated speed signal. As MPCC is model-dependent, saturation or temperature variations may affect the dynamic response of the motor. The speed utilized in MPCC was estimated from the adaptive mechanism, and the flux used was based on (3c). Based on the aforementioned equation of state (15), the mathematical model of the defined sensorless control algorithm was modeled in Matlab/Simulink. The model consists of three phase-two level six-switch inverters, dq-coordinate transformation, automatic speed regulator, predictive model controller, and adaptive observer. The adjustable model was continuously updated according to stator phase current estimates utilizing the adaptive mechanism. Modelling of proposed sensorless design is shown in Fig. 15. To show the effectiveness of proposed design, the design algorithm is compared with conventional MRAS

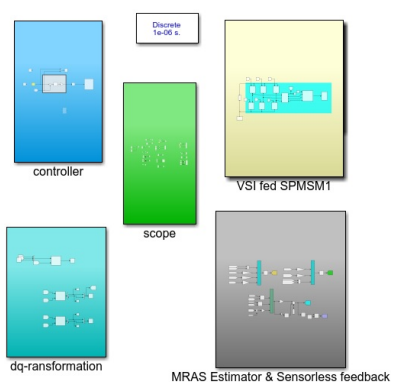

(a) Control Design

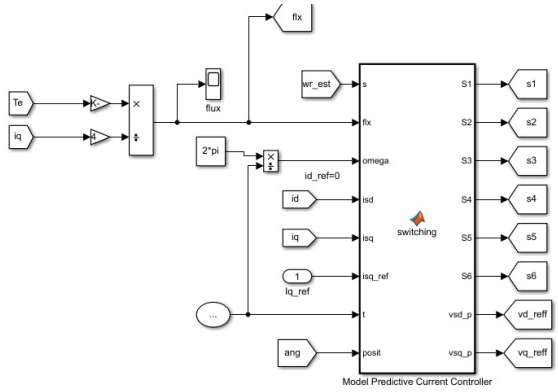

(b) Current Controller

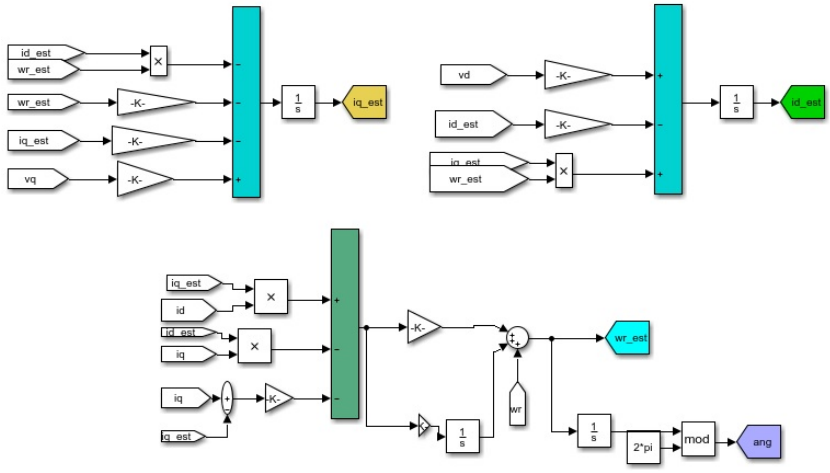

(c) Sensorless Speed design

Figure 15: Modelling of Proposed Design.

sensorless speed control with same parameter values as given in Table 2. The comparison results are shown in Fig. 16-24. Initially at low speed range from 180rpm to 360rpm is tested and shown in Fig. 16-17 The total simulation time is 2s. At low speed the steady state errors are obvious in traditional control design while the proposed design shows good response with no steady-state error and and convergence rate is fast in contrast to conventional design. After low speed

Table 2: Simulation Parameters of SPMSM.

Parameter	Value
Ts	1 μs
Stator resistance(R_s)	2.875Ω
Stator inductance(L_s)	8.5 mH
Moment of inertia(J)	0.0008 kgm^2
Flux	0.175 Wb
Poles Pairs (p)	4
Vdc	500 v
K_{ps}/K_{is}	30/4

the control design is tested for variable speed from 0 to 1200 rpm. The reference shaft speed changes from 0 rpm to 400 rpm at 0.1 s under the 2 Nm load torque. The load torque changes from 2 Nm to 5 Nm at 0.6s. under the load changes the tracking of estimated speed to actual speed is fast with no overshoot and steady state error in the design approach as compared to conventional sensorless speed control. The ripples across the torque is tremendously reduce in the proposed design. With utilizing MPCC the harmonic distortion across the phase current is reduced as compared to conventional PI current controller, the comparison of harmonic distortion under the various speed and load is shown.

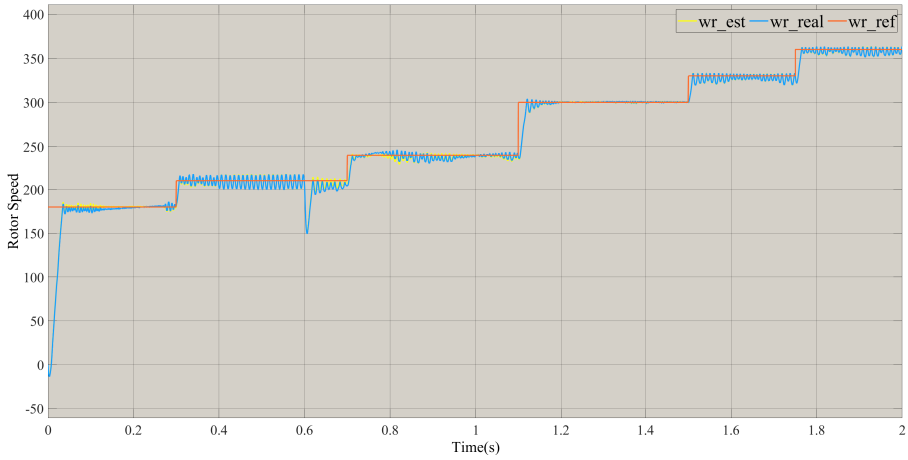

Figure 16: Low speed sensorless control based on conventional MRAS technique.

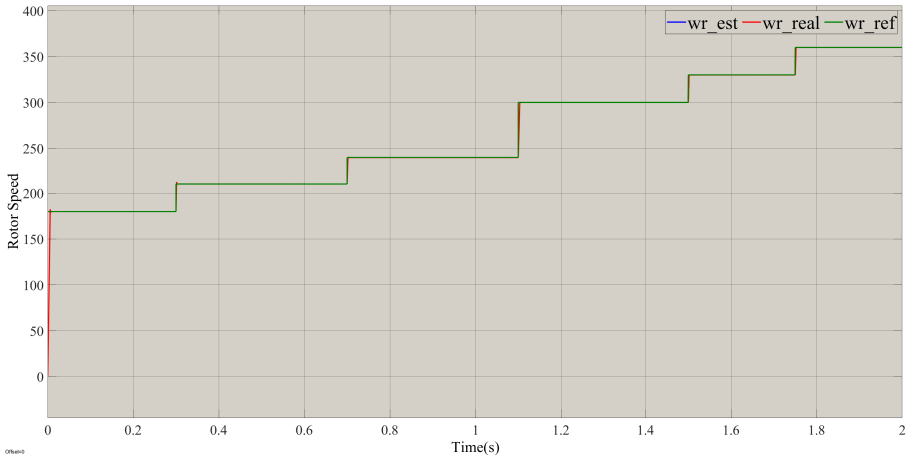

Figure 17: Low speed sensorless control based on proposed MRAS technique.

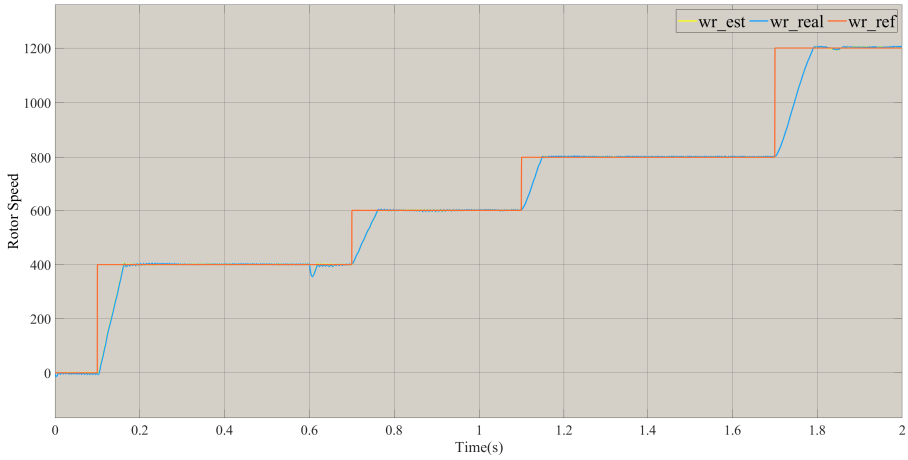

Figure 18: Sensorless speed response based on conventional MRAS technique.

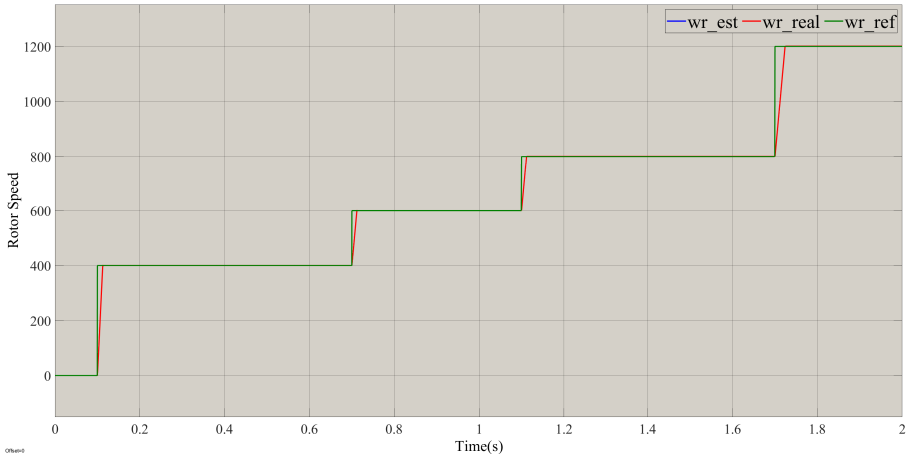

Figure 19: Sensorless speed response based on proposed MRAS technique.

Figure 20: Torque response based on conventional MRAS technique.

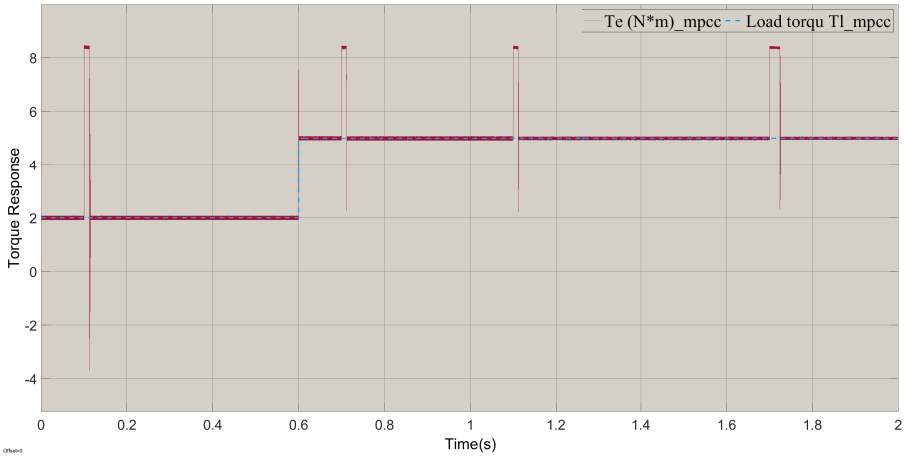

Figure 21: Torque response based on proposed MRAS technique.

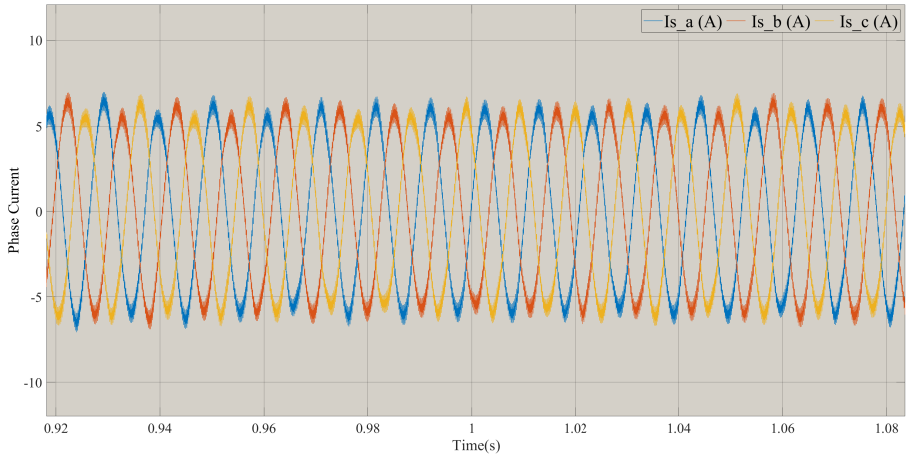

Figure 22: Motor phase current based on conventional MRAS technique.

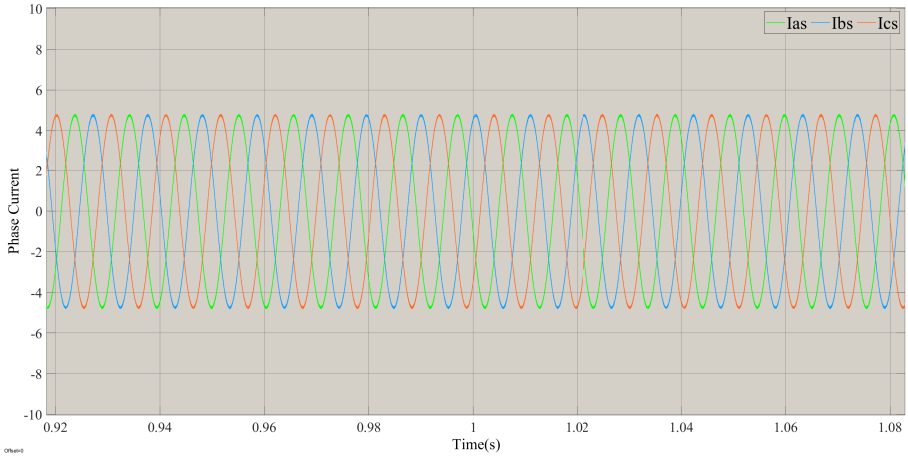

Figure 23: Motor phase current based on proposed MRAS technique.

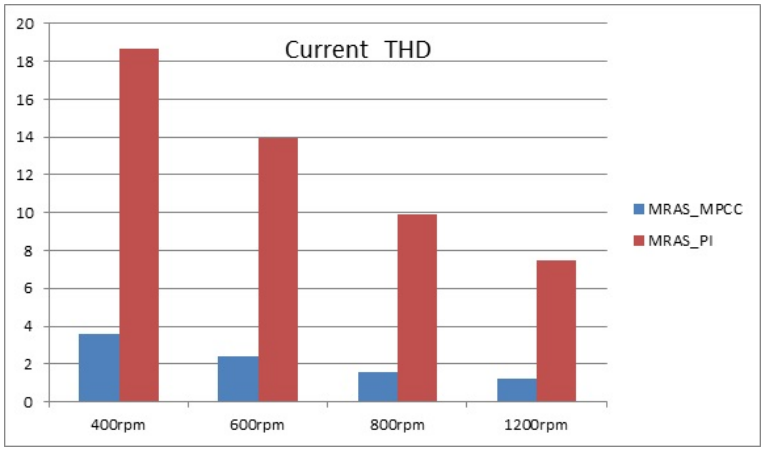

Figure 24: Harmonic distortion of proposed and conventional sensorless control.

The experiment has been carried out to verify the speed control at wide speed operation range.The overall speed response of design approach is shown in Fig. 25. Initially, a 5 Nm torque was applied to SPMSM. The tracking performance of the shaft speed response is quite good and fast. The estimated speed tracked the reference and actual speed quickly with minimum speed tracking error, as shown in Fig. 26. Under the loading condition, the motor showed excellent performance and fast dynamic response. At 1.1 s, the maximum speed of 1200 rpm was applied; and under the load, the estimated and actual speed reached the reference speed in 0.02 s. Similarly from the maximum negative speed to the positive speed region the controller take 0.074s.

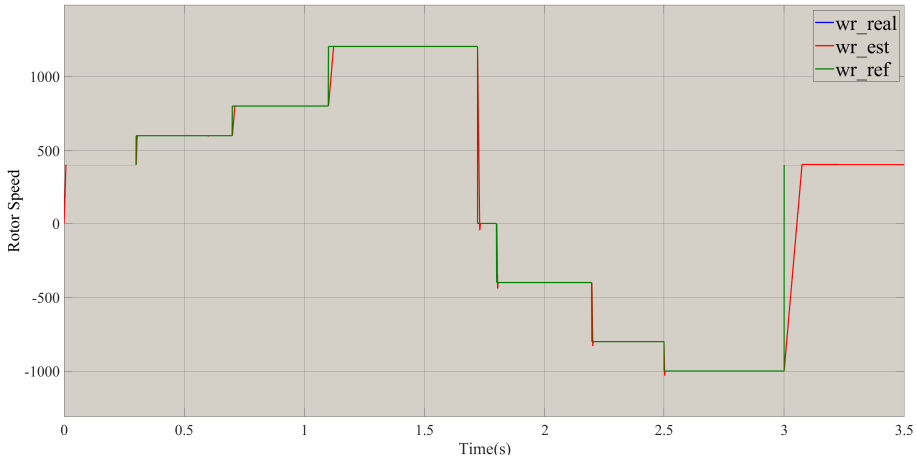

Figure 25: Estimated and real rotor shaft speed under different speed reference.

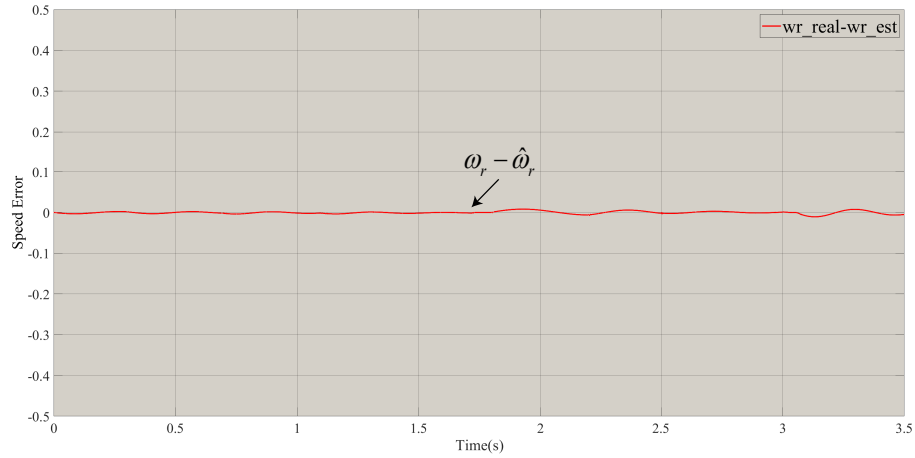

Figure 26: Speed error of sensorless algorithm.

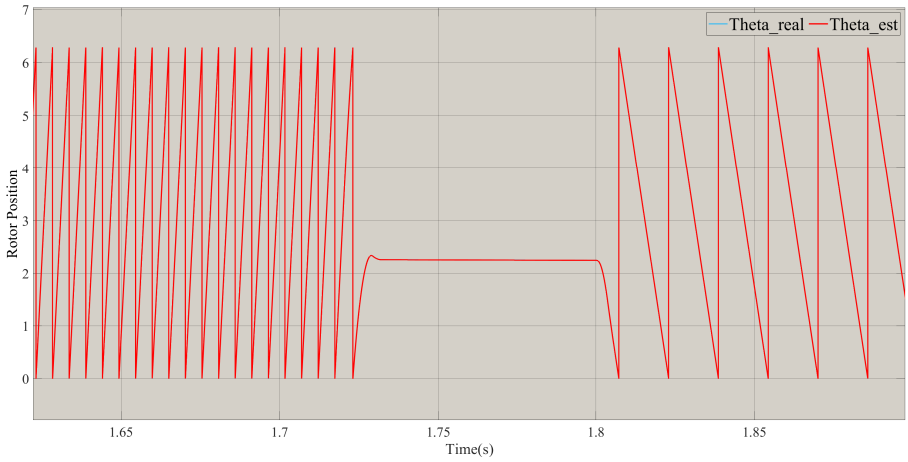

Figure 27: Estimated and real rotor shaft position.

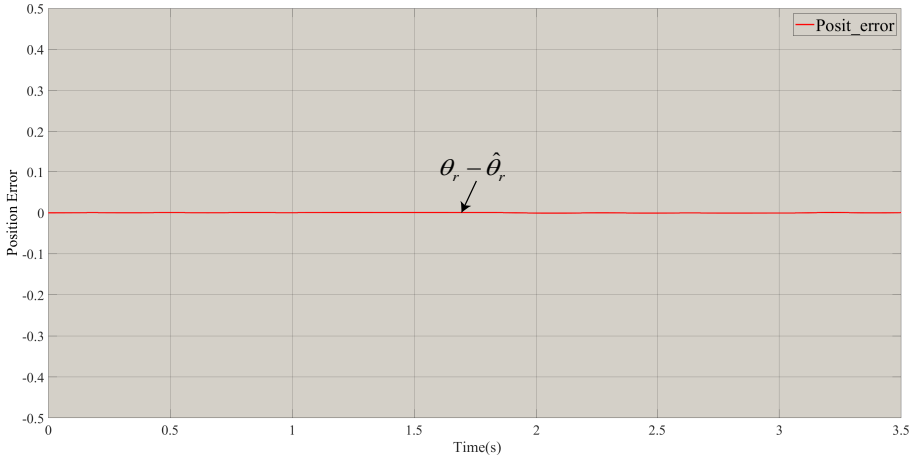

Figure 28: Position error of sensorless algorithm.

The steady-state performance of the system is stable with excellent performance at wide speed range operation. The estimated rotor shaft position obtained from the integration of the estimated shaft speed is shown in Fig. 27 along with the actual rotor position. The shaft position error signal is shown

in Fig. 28. Simulation results show that the shaft estimated position converged to the measured position very quickly. The instantaneous torque for encoder-less control of SPMSM is shown in Fig. 29. Under the loading condition, the tracking performance of the system was fast. At 0.6s when the load torque of 12Nm was applied. The results show that the torque reached to the rated value in 0.60126 s. The ripple across the torque was minimized with improved steady-state performance. The calculated flux is shown in Fig. 30 with minimum distortion under the loading condition.

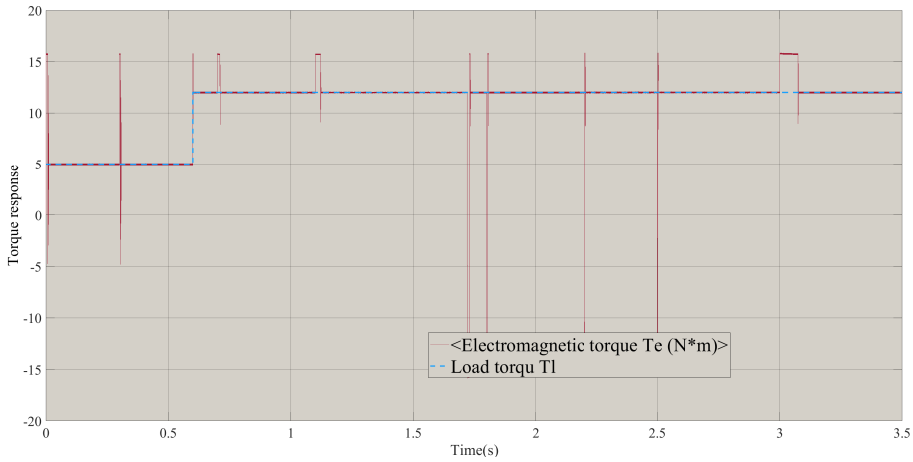

Figure 29: Torque response of SPMSM.

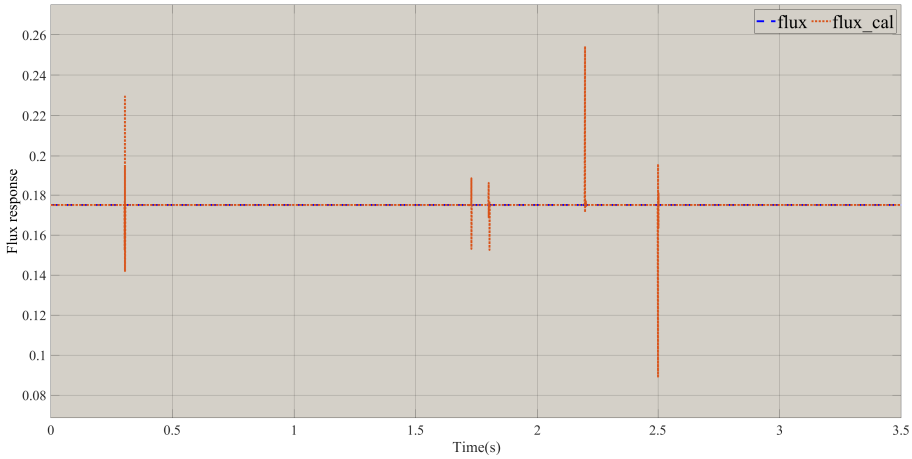

Figure 30: Flux response of SPMSM.

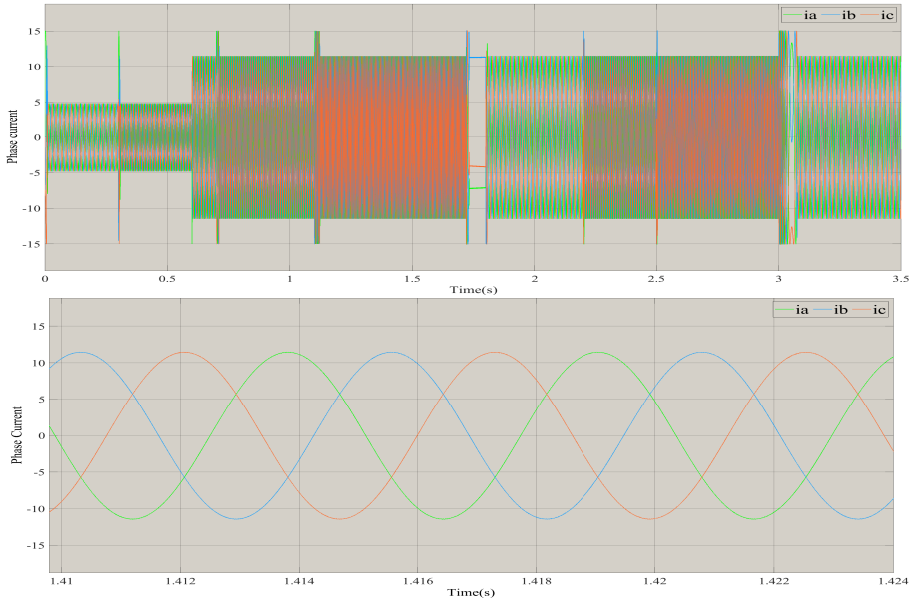

Figure 31: Three-phase motor current response.

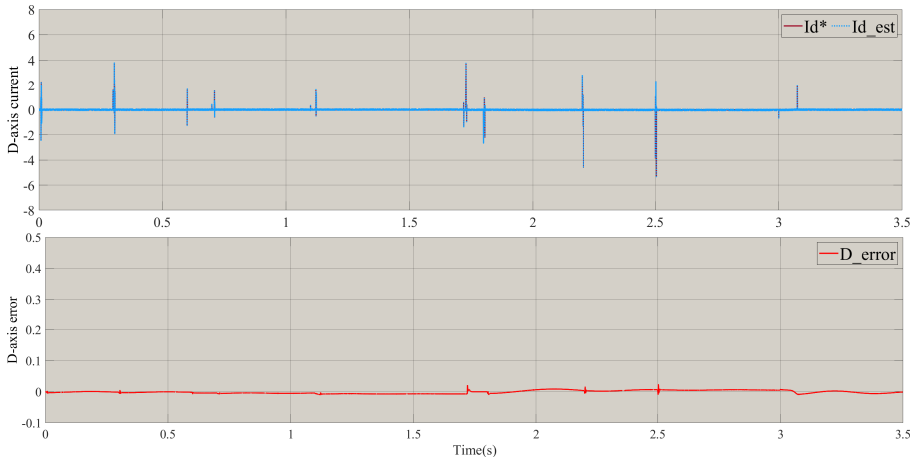

Figure 32: D-axis estimated and measured currents and error.

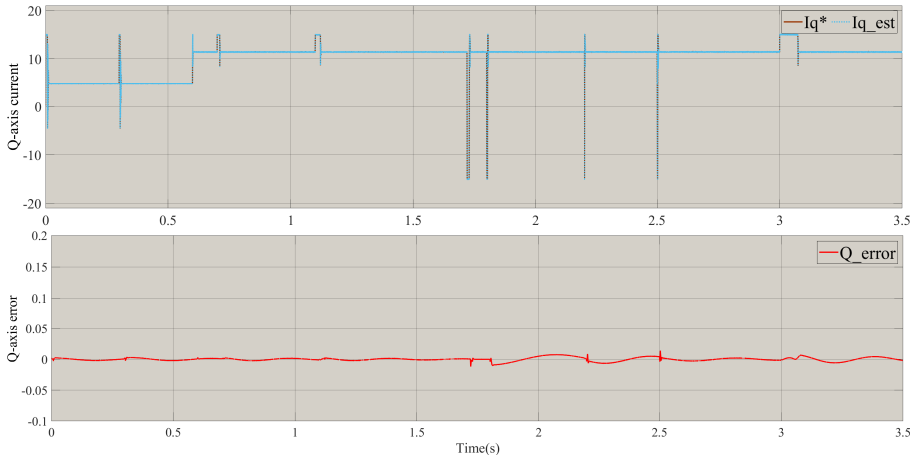

Figure 33: Q-axis estimated and measured currents and error.

The current response of the motor drive is shown in Fig. 31. It can be seen that the ripple across the three-phase currents were significantly reduced at wide speed range operation under the model predictive control mechanism. The dq-axis measured and estimated currents, and their errors are shown in Fig. 32

and 33. The MPCC showed fast tracking performance of the reference current to the measured current based on a prediction mechanism using optimal VV. The dq current response of the reference and adjustable is accurate with minimal steady-state error. The results verified that the proposed sensorless speed control algorithm can attain steady-state performance. Moreover, the overall dynamic response of motor drive is fast and robust.

V. CONCLUSION

The aim of the paper is to design a nonlinear current controller along side with adoptive mechanism to achieve efficient and dynamic sensorless speed control performance of SPMSM.

Based on traditional PI current controller the sensorless speed control design is modelled and implemented and at various speed and load condition the response of the motor derive is observed. Due to cascaded design the conventional PI current controller are very sensitive to parameter variation along with reference speed and load disturbance. The PI gain values are selected such that closed loop bandwidth is larger than the speed bandwidth. Due to these limitations the response of motor derive at low speed has steady state error with increase in rise time at high speed.

An MRAS based on FCS-MPCC was developed and implemented. The proposed algorithm is designed to enhance the encoder-less speed control performance of SPMSM under wide speed operation range, and reduce ripples across the current and torque under transient conditions. The proposed control design has better adaptability from the start, the speed and load torque variation of SPMSM. The steady-state performance of the sensorless speed control algorithm was proved by its fast dynamic response. The control performance of the developed scheme was verified through simulation under transient conditions. The response time of the system is very fast. The numerical analysis confirmed the feasibility and efficacy of the proposed adaptive control algorithm, and the simulation results verified the performance of the designed model. From the simulation results, we concluded that the proposed MRAS based on FCS-MPCC has fast dynamic response, is stable under various loading conditions,

and demonstrates the robustness of sensorless control. Furthermore, the steps of designing the controller based on Popov criterion doen't required expert experience and the adaptive law is by changing the function satisfying Popov's integral inequality. To summarize the analysis of proposed design following statement are observed.

- Reduce steady-state error and increase robustness.
- Effectively estimate the shaft speed and position.
- The reverse speed estimate do not require special design problem like speed sign computation near zero speed as compared to other sensorless control design.
- Minimize the harmonic distortion across the motor phase current.
- Achieve very fast current and torque response with short transient period.
- The convergence rate to desire speed reference is fast and accurate.
- Eliminate the need of cascaded linear controller that are sensitive to parameter perturbation.
- Increase the efficiency of the system and reduce system computational complexity.
- With Popov's stability criterion the proposed design is verified.
- The proposed hybrid control design is efficient for sensorless speed control and improve the system reliablity and increase robustness.

PUBLICATIONS

A. Conferences

1. M. Usama and J. Kim, "Vector Control Algorithm Based on Different Current Control Switching Techniques for Ac Motor Drives," in *E3S Web of Conferences*, EDP Sciences, vol. 152, 2020, p. 03 009. DOI: 10.1051/e3sconf/202015203009.

2. M. Usama and K. Jaehong, "Simplified Model Predicted Current Control Method for speed control of Non-Silent Permanent Magnet Synchronous Motors," in *2020 3rd International Conference on Computing, Mathematics and Engineering Technologies (iCoMET)*, IEEE, 2020, pp. 1–5.

3. M. Usama and K. Jaehong, "Sensorless Speed Control of Non-silent Permanent Magnet Synchronous Motoer Established on a Nonlinear Observer Approach," in *2020 IEEE 9th International Power Electronics and Motion Control Conference (IPEMC2020-ECCE Asia)*, IEEE, 2020, [Publication in Progress].

A Appendix

In this appendix the proof for the stability of feed-forward transfer function of the dynamic system is derived.

For the stability the feed-forward transfer function of the system is strictly lemma positive real [25]. the transfer function from state space form of dynamic system (2) is written as

$$G_s = C[Is - A]^{-1}B + D. \tag{A.1}$$

where (A,C) is observable and (A,B) is controllable, as A is the square matrix also called stable matrix(or sometime a Hurwitz matrix) if the eigenvalues of A has negative real part, then the dynamic of the system has a hurwitz transfer function and makes G(s) stable. To show the stability of transfer function the set of three equation must be satisfied that are given as [31]:

$$\begin{cases} A^T P + AP = -L^T L. \\ PB = C^T - L^T W. \\ W^T W = D + D^T. \end{cases} \tag{A.2}$$

if the above mentioned equations are satisfied then G(s) is equivalent to Lemma Positive real.

$$G(s) + G(s^*)^T \geq 0. \tag{A.3}$$

Let write $[Is - A]^{-1} = \phi(s)$, so (A.3) can rewrite as:

$$C\phi(s)B + D + D^T + C^T \phi(s^*)^T B^T. \tag{A.4}$$

from (A.2) equation become

$$C\phi(s)B + W^T W + C^T \phi(s^*)^T B^T. \tag{A.5}$$

so from (A.2)

$$C\phi(s)B + W^TW + [PB + L^TW]\phi(s^*)^TB^T. \tag{A.6}$$

$$C\phi(s)B + W^TW + PB\phi(s^*)^TB^T + L^TW\phi(s^*)^TB^T. \tag{A.7}$$

now for c as $C = P^TB^T + LW^T$

$$P^TB^T\phi(s)B + LW^T\phi(s)B + W^TW + PB\phi(s^*)^TB^T + L^TW\phi(s^*)^TB^T. \tag{A.8}$$

as P is symmetric matrix so $P = P^T$ so we get $P^TB^T\phi(s)B + PB\phi(s^*)^TB^T$ by simplification

$$B^T\phi(s^*)^T[P(Is - A)]\phi(s)B + B[P(Is - A)^{-1}]\phi(s^*)^TB^T\phi(s). \tag{A.9}$$

$$B^TB\phi(s^*)^T\phi(s)[(s + s^*)P - AP - A^TP]. \tag{A.10}$$

now

$$B^TB\phi(s^*)^T\phi(s)[(s + s^*)P) + L^TL]. \tag{A.11}$$

$$B^TB\phi(s^*)^T\phi(s)(s + s^*)P + L^TLB^TB\phi(s^*)^T\phi(s). \tag{A.12}$$

put it in (A.8)

$$B^TB\phi(s^*)^T\phi(s)(s + s^*)P + LW^T\phi(s)B + W^TW + L^TLB^TB\phi(s^*)^T\phi(s) + L^TW\phi(s^*)^TB^T. \tag{A.13}$$

$$G(s) + G(s^*)^T = \underbrace{B^TB\phi(s^*)^T\phi(s)(s + s^*)P}_{P\ is\ positive\ symmetric\ matrix} + \underbrace{(W^T + L^T\phi(s^*)^TB^T)(W + L\phi(s)B)}_{square\ matrix\ and\ always\ positive}. \tag{A.14}$$

$$So\ G(s)\ is\ positive\ real. \tag{A.15}$$

so

$$G(s) + G(s^*)^T \geq 0. \tag{A.16}$$

for all $R_e|s| \geq 0$

by this derivation the transfer function is strictly lemma positive real.

REFERENCES

[1] A. R. Beig and V. T. Ranganathan, "A novel csi-fed induction motor drive," *IEEE Transactions on Power Electronics*, vol. 21, no. 4, pp. 1073–1082, 2006.

[2] N. Senthil Kumar and K. Saravanan, "Speed control of pmsm drive using vsi," in *30th Annual Conference of IEEE Industrial Electronics Society, 2004. IECON 2004*, vol. 1, 2004, 888–895 Vol. 1.

[3] K. Nam, *AC motor control and electric vehicle applications*. New York, USA: CRC Press, 2010, ch. Permanent Magnet AC Motors.

[4] I. Boldea, "Control issues in adjustable speed drives," *IEEE Industrial Electronics Magazine*, vol. 2, no. 3, pp. 32–50, 2008.

[5] A. S. Mohamed, M. S. Zaky, A. S. Z. E. Din, and H. A. Yasin, "Comparative study of sensorless control methods of pmsm drives," *Innovative Systems Design and Engineering*, vol. 2, pp. 44–66, 2011.

[6] S. Sul, Y. Kwon, and Y. Lee, "Sensorless control of ipmsm for last 10 years and next 5 years," *CES Transactions on Electrical Machines and Systems*, vol. 1, no. 2, pp. 91–99, 2017.

[7] H. Kim, J. Son, and J. Lee, "A high-speed sliding-mode observer for the sensorless speed control of a pmsm," *IEEE Transactions on Industrial Electronics*, vol. 58, no. 9, pp. 4069–4077, 2011.

[8] O. C. Kivanc and S. B. Ozturk, "Sensorless pmsm drive based on stator feedforward voltage estimation improved with mras multiparameter estimation," *IEEE/ASME Transactions on Mechatronics*, vol. 23, no. 3, pp. 1326–1337, 2018.

[9] Z. Qiao, T. Shi, Y. Wang, Y. Yan, C. Xia, and X. He, "New sliding-mode observer for position sensorless control of permanent-magnet synchronous motor," *IEEE Transactions on Industrial Electronics*, vol. 60, no. 2, pp. 710–719, 2013.

[10] S. Barkat, A. Tlemçani, and H. Nouri, "Noninteracting adaptive control of pmsm using interval type-2 fuzzy logic systems," *IEEE Transactions on Fuzzy Systems*, vol. 19, no. 5, pp. 925–936, 2011.

[11] Z. Xingming, W. Xuhui, Z. Feng, G. Xinhua, and Z. Peng, "Wide-speed-range sensorless control of interior pmsm based on mras," in *2010 International Conference on Electrical Machines and Systems*, 2010, pp. 804–808.

[12] Y. Cai and H. Ma, "Sensorless speed control of pmsm based on improved mras method," in *2017 China International Electrical and Energy Conference (CIEEC)*, 2017, pp. 210–214.

[13] D. Casadei, F. Profumo, G. Serra, and A. Tani, "Foc and dtc: Two viable schemes for induction motors torque control," 2002.

[14] L. Zhong, M. F. Rahman, W. Y. Hu, and K. W. Lim, "Analysis of direct torque control in permanent magnet synchronous motor drives," *IEEE Transactions on Power Electronics*, vol. 12, no. 3, pp. 528–536, 1997.

[15] S. Qin and T. Badgwell, "A survey of industrial model predictive control technology.," *Control Eng. Pract*, vol. 11, pp. 733–764, 2003.

[16] E. J. Fuentes, J. Rodriguez, C. Silva, S. Diaz, and D. E. Quevedo, "Speed control of a permanent magnet synchronous motor using predictive current

control," in *2009 IEEE 6th International Power Electronics and Motion Control Conference*, 2009, pp. 390–395.

[17] Yongchang Zhang and Xianglong Wei, "Torque ripple rms minimization in model predictive torque control of pmsm drives," in *2013 International Conference on Electrical Machines and Systems (ICEMS)*, 2013, pp. 2183–2188.

[18] Y. Zhu, J. Yin, and G. Xu, "A comparative study of mpcc and mptc in pmsm drive system," in *2018 IEEE 2nd International Conference on Circuits, System and Simulation (ICCSS)*, 2018, pp. 36–40.

[19] M Tang and S. Zhuang, "On Speed Control of a Permanent Magnet Synchronous Motor with Current Predictive Compensation.," *Energies*, vol. 12, p. 65, 2019.

[20] B. Gmati, S. K. El Khil, and I. Slama-Belkhodja, "Improved mpc for pmsm drives to reduce switching losses," in *2017 International Conference on Green Energy Conversion Systems (GECS)*, 2017, pp. 1–8.

[21] Y. Zhang, D. Xu, J. Liu, S. Gao, and W. Xu, "Performance improvement of model-predictive current control of permanent magnet synchronous motor drives," *IEEE Transactions on Industry Applications*, vol. 53, no. 4, pp. 3683–3695, 2017.

[22] K. Astrom and B Wittenmark, *Adaptive control*. Mineola, New York, USA: Dover Publication, 2008.

[23] Young Sam Kim, Sang Kyoon Kim, and Young Ahn Kwon, "Mras based sensorless control of permanent magnet synchronous motor," in *SICE 2003*

Annual Conference (IEEE Cat. No.03TH8734), vol. 2, 2003, pp. 1632–1637.

[24] Rasvan and Vladimir, "Popov theories and qualitative behaviour of dynamic and control system," *European Journal of Control*, vol. 8, pp. 190–199, 2002.

[25] K. Liu, Q. Zhang, Z. Zhu, J. Zhang, A. Shen, and P. Stewart, "Comparison of two novel MRAS strategies for identifying parameters in permanent magnet synchronous motors," *Int. J. Autom. Comput*, vol. 7, pp. 516–524, 2010.

[26] I. Landau, "A hyperstability criterion for model reference adaptive control systems," *IEEE Transactions on Automatic Control*, vol. 14, no. 5, pp. 552–555, 1969.

[27] A. Khlaief, B. Mohamed, and C. Abdelkader, "A MRAS-based stator resistance and speed estimation for sensorless vector controlled IPMSM drive," *Electr. Power Syst. Res*, vol. 108, pp. 1–15, 2014.

[31] Chengshan Xiao and D. J. Hill, "Generalizations and new proof of the discrete-time positive real lemma and bounded real lemma," *IEEE Transactions on Circuits and Systems I: Fundamental Theory and Applications*, vol. 46, no. 6, pp. 740–743, 1999.

ACKNOWLEDGEMENTS

I extend my heartfelt thanks to Almighty ALLAH who showered his blessing upon me and gave me strength,courage and patience for completion of this paper. I would like to express my sincere gratitude to my family and friends for kind support throughout my research.

I am grateful to my advisor, Dr.Jaehong Kim, for providing tremendous levels of support over the last two years. His mentoring, encouragement and persistence have shaped my own engineering problem-solving approach. His profound knowledge, hard working and enormous experience in research, and great patience in teaching inspired and helped me to gradually develop critical thinking. It has been a sincere privilege to study under his direction. Thanks are due to my committee, Dr.Yong-Jae Kim, Dr.Youn-Ok Choi for their involvement, feedback and the time that they spent reviewing this thesis.